Interaction of Drive Modulation and Cable Parameters on AC Motor Transients

Russel J. Kerkman, *Senior Member, IEEE,* David Leggate, *Member, IEEE,* and Gary L. Skibinski, *Member, IEEE*

***Abstract*— This paper investigates overvoltage transients on ac induction motors when connected through a cable of arbitrary length to a variable frequency drive (VFD) consisting of a pulsewidth modulation (PWM) inverter with insulated gate bipolar transistor (IGBT) power devices. Factors contributing to a motor overvoltage transient equal to a theoretical twice dc bus voltage are first described using existing transmission line analysis. A critical cable distance l_c is defined where this 2-pu overvoltage occurs. However, literature is lacking on how motor voltage transients >2-pu bus voltage and up to 3–4 pu are generated. This phenomenon is observed on *all* PWM inverters with output cable lengths greater than l_c distance. Contributing factors to the >2-pu overvoltage phenomenon are investigated by exploring the complex interaction between drive modulation techniques, carrier frequency selected, cable natural frequency of oscillation, cable high-frequency damping losses, and, to a lesser extent, inverter output rise time. Theoretical calculations of cable frequency and damping are correlated with simulation and experimental results. Novel modifications to the PWM modulator, as well as external hardware apparatus, are proposed solutions to the >2-pu overvoltage problem; both are simulated and experimentally confirmed.**

***Index Terms*— Cable impedance, pulse elimination technique (PET), transient overvoltages, voltage reflection.**

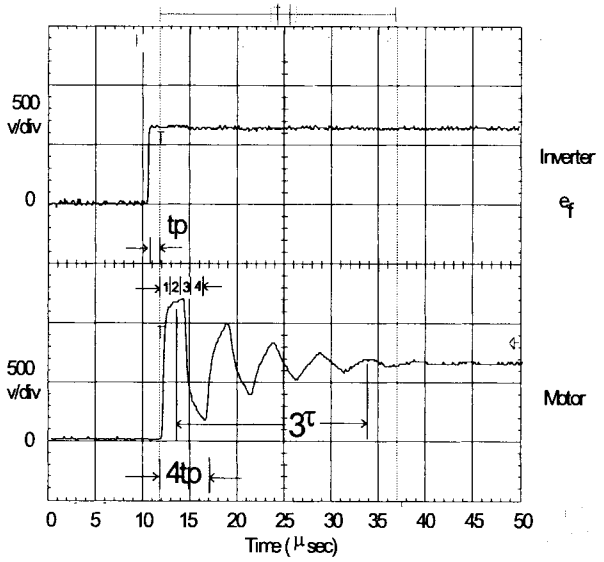

Fig. 1. Experimental results: transient charging of 500 ft #12-gauge PVC motor cable.

I. Introduction

SYSTEM efficiency and productivity improvements attainable through variable frequency drives (VFD's) have meant an increasing segment of low-voltage standard ac induction motors are now operated with pulsewidth modulation (PWM) voltage–source inverters from 0.1 to 800 kW using insulated gate bipolar transistors (IGBT's) as the preferred semiconductor switching device. IGBT switching speed (50–400 ns) is an order of magnitude faster than bipolar junction transistors (BJT's), so that drive switching efficiency is increased, drive package heat sinks are reduced, and higher carrier frequencies (f_c) are possible. Higher f_c improves current waveform quality, as well as reducing audible noise in motor laminations.

However, ac motor transient overvoltages resulting from drive-motor-cable dynamic response to inverter pulse voltages have steadily increased in magnitude as semiconductor rise and fall switching times have decreased from gate turn-off (GTO) devices, to BJT's, and presently to IGBT's. This trend has occurred while the peak transient overvoltage capability of the motor's dielectric insulation system has remained unchanged at $\approx$ 1200 V_{pk} [1]. Previously, cable application lengths had to exceed 1000–2000 ft for GTO drives and 500–1000 ft for BJT drives before exceeding motor overvoltage dielectric capability. Presently, IGBT drives may create overvoltages that exceed the safe motor level for cable lengths as low as 50–200 ft. Thus, a high percentage of VFD applications are now suspect and provide a motivating factor to characterize how these destructive ac motor transient voltages are generated.

The objective of this paper is to first review factors contributing to motor transient voltages that are <2-pu (1 pu = dc bus voltage). Second, this paper will investigate factors contributing to the more complex problem of motor overvoltages >2-pu bus voltage by using basic physical equations, modeling, simulation, and experimental results. Third, hardware and software solutions that restrict motor overvoltage to safe operating levels will be proposed.

II. Factors Contributing to Motor Overvoltage <2-pu Bus Voltage

Transmission line literature exists that describes transient overvoltages with zero initial charge on cables, as shown in Fig. 1. techniques such as graphical traveling-wave analysis [2], Bewley lattice diagrams [3], Smith chart analysis [4], and standing-wave analysis [1] are available. Factors contributing

Paper IPCSD 97–06, approved by the Industrial Drives Committee of the IEEE Industry Applications Society for presentation at the 1996 Industry Applications Society Annual Meeting, San Diego, CA, October 6–10. Manuscript released for publication January 6, 1997.

The authors are with the Standard Drives Business, Rockwell Automation–Allen Bradley Company, Mequon, WI 53092 USA.

Publisher Item Identifier S 0093-9994(97)02946-0.

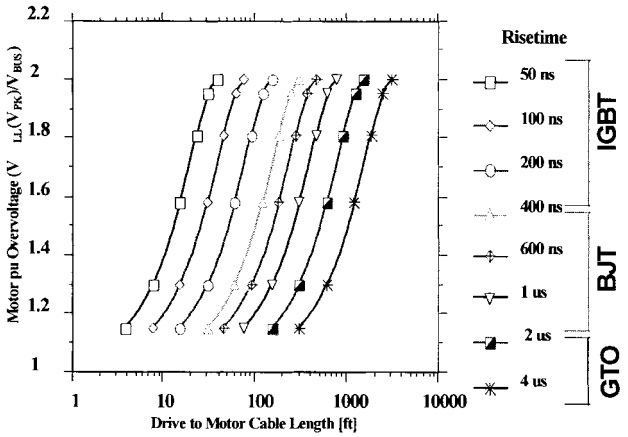

Fig. 2. Motor terminal voltage for uncharged cable.

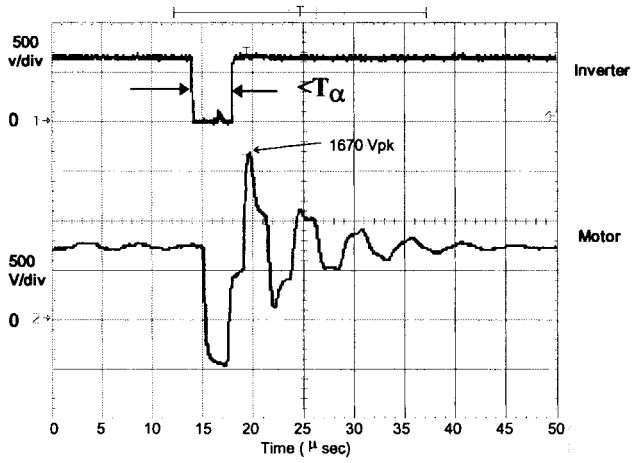

Fig. 3. PWM and the effects of double pulsing.

to motor overvoltage are cable length and cable-to-motor surge impedance matching, but magnitude and rise time of the PWM output voltage pulses are the predominant factors in this mode, as shown in Fig. 2 and explained in [1]. Carrier frequency selection has little effect on motor overvoltage in this mode. Fig. 2 provides a worst-case design methodology to estimate motor terminal voltage for an initially uncharged cable condition and assuming complete cable-to-motor surge impedance mismatch. This allows classical lossless transmission line analysis, treating the motor end as an open-circuited line with full voltage reflection taking place. A critical cable distance l_c may be defined where this full theoretical 2-pu overvoltage reflection occurs.

III. Factors Contributing to Motor Overvoltage >2-pu Bus Voltage

There are certain modes in a PWM modulation cycle that, combined with long cable lengths, can lead to motor stress greater than the theoretical 2-pu overvoltage with magnitudes of 3-pu to 4-pu bus voltage possible. Fig. 3 shows such a condition, where the last cable transient has not fully decayed before the application of the next pulse, so that a residual trapped cable charge condition exists that may lead to 3-pu overvoltage. The effects of these transients >2-pu are investigated in [5] and shown to have adverse effects on motor dielectric life. A typical pu overvoltage versus cable length curve experimentally derived is shown in Fig. 4, with the l_c distance marked.

In contrast to the conclusions of [6], it is seen that carrier switching frequency and modulation technique have a predominant effect on motor overvoltage in this mode, due to the spacing of modulation pulses while inverter rise time has a lesser effect in this mode.

The cable's natural oscillation frequency has a large influence on cable ac damping resistance which, in turn, has an effect on how much residual charge is trapped on the cable before the next inverter pulse. A good source on high-frequency cable losses has not been found according to [2]. Thus, a technical investigation, including the physical equations describing cable oscillation frequency and cable ac high

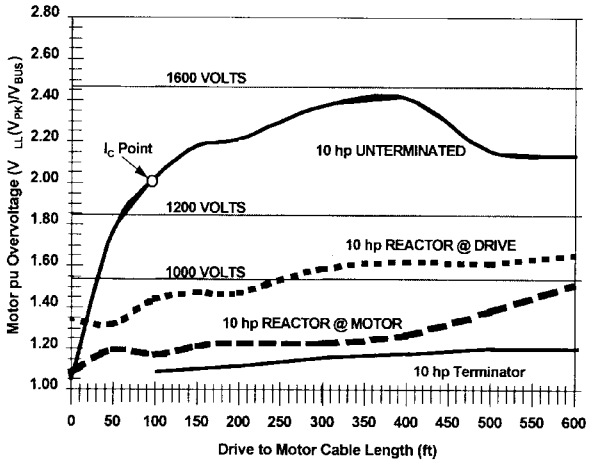

Fig. 4. Terminal voltage experimental data at 480 V.

frequency damping resistance, is derived and experimentally verified in this section.

A. Oscillation Frequency of Reflected Wave

Fig. 1 shows a single PWM output voltage pulse (e_f) of dc bus magnitude ($V_{\rm bus}$) traveling down two conductors of a bundled initially uncharged cable. Voltage oscillations around $V_{\rm bus}$ result once the incident wave e_f reaches the motor terminals. Oscillation frequency at the motor terminals is solely determined by cable characteristics and independent of *any* drive or motor characteristics, including pulse rise time and horsepower size. The first oscillation has a theoretical peak of $2V_{\rm bus}$ and a theoretical minimum of zero voltage. Successive oscillations have smaller peak voltage excursions around the $V_{\rm bus}$ pulse level, due either to cable resistance damping or reflection coefficient mismatch occurring at both drive and motor ends. Cable oscillation frequency is an important aspect in the creation of >2-pu motor overvoltage transients and is analyzed using two-conductor transmission line theory. Cable resistance does modify wave velocity slightly. Therefore, lossless line models to estimate oscillation frequency (f_o) are valid.

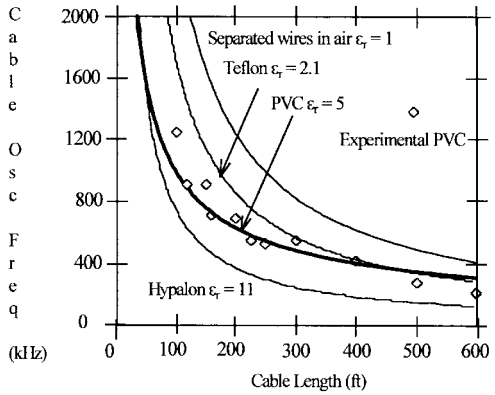

Fig. 5. Oscillation frequency versus cable length.

Inverter output pulse (e_f) travels from drive to motor over cable length distance (a) during cable propagation time (t_p), as shown in Fig. 1. All points in the pulse envelope travel at the same velocity ν and pulse shape is propagated without distortion down the line. The $\pm$ sign of (1) indicates that both forward and reverse waves travel at the same velocity. Wave propagation velocity is a function of cable inductance per unit length (L_o) and cable capacitance per unit length (C_o) [1]. Propagation velocity may also be defined using permeability (μ) and permittivity (ε) of the dielectric material between conductors [7]. Substitution of free space constants $\mu = \mu_0\,\mu_r$ and $\varepsilon = \varepsilon_0\,\varepsilon_r$ and setting $\mu_r = 1$ for cable insulations, results in ν expressed as a function of relative dielectric constant ε_r and speed of light ($c = 3.0 \times 10^8$ m/s) [3]. Velocity ν is measured at 1.524×10^8 m/s (50% of c) using $\partial x = a = 162$ m (500 ft) and measured t_p of 1 μs from Fig. 1. Velocity ν is also estimated at near 50% of c from (1) using typical $\varepsilon_r = 4.5$ for a three-conductor bundled polyvinylchloride (PVC) insulated wire. Velocity ν varies from a low of 32% c for Hypalon ($\varepsilon_r \approx$ 9–11) bundled wires to 70% c for Teflon ($\varepsilon_r = 2.0$) bundled wires. Velocity $v = c$ when widely separated conductors are used, since $\varepsilon_r = 1.0$. The following analysis is valid for a typical case where IGBT voltage risetime $\leq$ cable t_p time:

$$v = \frac{\partial x}{\partial t} = \pm\frac{1}{\sqrt{L_o C_o}} = \frac{1}{\sqrt{\mu\varepsilon}} = \frac{c}{\sqrt{\varepsilon_r}}. \tag{1}$$

The cycle time of the traveling wave relates the cable length to ν [7]. To complete one oscillation cycle requires the wave to traverse a four times—$T_{\text{cycle}} = 4t_p$. Thus, f_o may be expressed in terms of cable length and cable characteristics.

Oscillation frequency is inversely proportional to cable length from (2) and graphed in Fig. 5 with the experimental data points for PVC:

$$f_o = \frac{1}{T_{cycle}} = \frac{1}{4t_p} = \frac{\nu}{4a} = \frac{1}{4a\sqrt{L_o C_o}}. \tag{2}$$

Thus, high oscillation frequencies occur at short cable lengths. Fig. 5 shows agreement between calculated line and experimental data points. The f_o of Fig. 1 is 250 kHz, which agrees with data of Fig. 5. Fig. 5 also shows calculated f_o curves when bundled cables of various insulation types are used.

Cable construction, insulation type, and conductor spacing all determine cable parameters L_o and C_o, which define cable wave velocity ν. A bundled cable construction compared to widely separated conductors ($\varepsilon_r = 1$) results in lower ν from (1) and, thus, a lower f_o from (2). The ε_r values of various wire insulation types also affect ν, which is directly proportional to f_o from (2).

B. Damping Time of Reflected Waves

Cable oscillation frequency indirectly affects damping characteristics of the overvoltage transient due to conductor ac resistance being increased as a result of skin $[K_{\text{skin}(f_o)}]$ and proximity (K_p) effects. Resistance losses produce a power loss in the forward PWM voltage pulse e_f, current pulse i_f, and the reflected wave pulses. Heat is dissipated in both the series conductor ac resistance r_s (Ω/unit length) and cable parallel insulation resistance r_p (Ω/unit length), a high ohmic value. The initial pulse amplitude (e_o) will be exponentially attenuated to its final value (e) dependent only on cable constants r_s, Z_o (where $Z_o = \sqrt{L_o/C_o}$), K_p, $K_{\text{skin}(f_o)}$, and cable distance x traveled:

$$\frac{e}{e_o} = \varepsilon^{-(r_s x/2Z_o)} = \varepsilon^{-(K_p K_{\text{skin}(f_o)}\, r_{\text{dc}} x/2Z_o)}. \tag{3}$$

Thus, tightly bundled phase conductors have greater damping than widely separated conductors, since Z_o of bundled cables is 80–150 Ω and is 10–20 times lower than for separated conductors [7]. Reflected waves traveling between the drive and the motor dampen quickly, since distance ($x = 4a$ in meters) is traveled during each successive oscillation cycle. Also, damping is greater in lower horsepower drives, since smaller gauge wires have higher dc resistance values in the r_s term.

Resistance r_s (ac Ω/conductor/m) is dependent on cable oscillation frequency and is increased above the dc value due to skin and proximity effects. Skin effect is due to the fact that internal inductance of a conductor is highest at the center and least at the edges. Thus, high-frequency current oscillating at f_o tends to crowd to the conductor surface, decreasing the apparent conductor area and increasing ac resistance. Proximity effect is due to magnetic fields of a neighboring adjacent conductor distorting and effectively reducing current flow area in the primary conductor. It is sensitive to conductor-to-conductor spacing. Proximity effect increases ac resistance by a factor of two ($K_p = 2$) in (3) for tightly bundled round conductor cables [8]. The skin effect factor $[K_{\text{skin}(f_o)}]$ in (3) is a function of frequency [3].

Skin depth of penetration (δ) is defined when conductor current density in the radial dimension is at the ε^{-1} value. Substitution of permeability (μ) and conductivity (σ) for copper results in $\delta_{\text{Cu}} = 0.0661/\sqrt{f_o}(m)$ [3]. The total amount of high-frequency power carried by the conductor can be described by the Poynting Vector equation ($P_\nu \propto \varepsilon^{-2\gamma/\delta}$) [3]. Substitution of $\gamma = \delta/2$ yields the radial depth beyond which minimal high-frequency power is transmitted. With $\gamma = \delta_{\text{Cu}}/2$, the expression for $K_{\text{skin}(f_o)}$ becomes [7]:

$$K_{\text{skin}(f_o)} = \frac{\frac{\pi\, d_o}{4}}{\pi\, d} = \frac{d_o}{2\delta} = \frac{d_o\sqrt{f_o}}{2\,(0.0661)}. \tag{4}$$

TABLE I
PREDICTED AND MEASURED CONDUCTOR AC RESISTANCE VERSUS FREQUENCY

Wire Gauge		#18		#8	
dc resistance [Ω/m]		0.01935		0.002132	
do diameter [m]		0.0012446		0.0037338	
ac resistance [Rac/Rdc]		Predicted	Measured	Predicted	Measured
Frequency [kHz]	10	1.4	2.3	4	3.4
	100	4.4	4	13	17
Frequency [MHz]	1	14	14	42	60

Finally, (5) expresses solid wire copper conductor ac resistance r_s as a function of cable oscillation frequency f_o that includes skin and proximity effects:

$$r_s = K_p K_{\text{skin}(f_0)} R_{\text{dc}} = K_p \left[\frac{d_o\sqrt{f_o}}{2(0.0661)}\right]\left(\frac{4\rho}{\pi d^2}\right) = \frac{K_p\, 16.61 * 10^{-8}\sqrt{f_o}}{d_o}. \quad (5)$$

Table I validates predicted r_s values with measured data versus frequency. Prediction of high-frequency r_s for large d_o wire is difficult, since the number and size of conductor strands is critical.

The time to damp reflected pulses to <5% of initial peak value is estimated by substituting $x = \nu t$, $\nu = 1/(L_oC_o)^{0.5}$ and $Z_o = (L_o/C_o)^{0.5}$ into (3). Reflected wave overvoltages are damped out in a 3τ time interval, with τ = one time constant $= (2L_o/r_s)$:

$$\frac{e}{e_o} = \varepsilon^{-(r_s x/2Z_o)} = \varepsilon^{-(r_s \nu t/2Z_o)} = \varepsilon^{-(r_s/2L_o)t} = \varepsilon^{-t/\tau}. \quad (6)$$

Fig. 6 graphs calculated 3τ times for bundled cables of various conductor gauges that include skin and proximity effect factors for r_s. A measured skin effect ($L_o \approx 91$ nH/ft at f_0 <1 kHz and 85 nH/ft atf_0 >100 kHz) was used for all bundled cables [8]. Measured 3τ time from Fig. 1 is $\approx$ 20 μs for 500 ft of #12-AWG bundled cable. Calculated f_o oscillation frequency is 250 kHz from Fig. 5, while calculated 3τ time from Fig. 6 is $\approx$ 18 μs. Measured and calculated 3τ times for wires of #18, #14, and #8 AWG were within 8%.

Fig. 6 shows typical 3τ damping times to reflected wave transients are between the dark solid lines corresponding to cable lengths of 600 ft ($\approx f_o = 200$ kHz) and 100 ft ($\approx f_o =$ 1 MHz). This figure shows skin effect ac resistance has a large influence on damping the reflected transients, as compared to the 60-Hz resistance. Fig. 5 also shows the shorter the cable, the higher the f_o and the faster the damping effect from the cable resistance. It is critical to have the reflected wave overvoltage transient oscillation decay to zero before the arrival of the next PWM pulse. For example, the $T\alpha$ time in Fig. 3 is less than 3τ, causing the overvoltage transient upon the arrival of the next PWM pulse. Therefore, T_{on} must be greater than $T_\alpha = 3\tau$. This prevents trapped line charge from causing a possible 3-pu overvoltage transient when PWM dwell times (*the time when the line-to-line voltage is zero*)

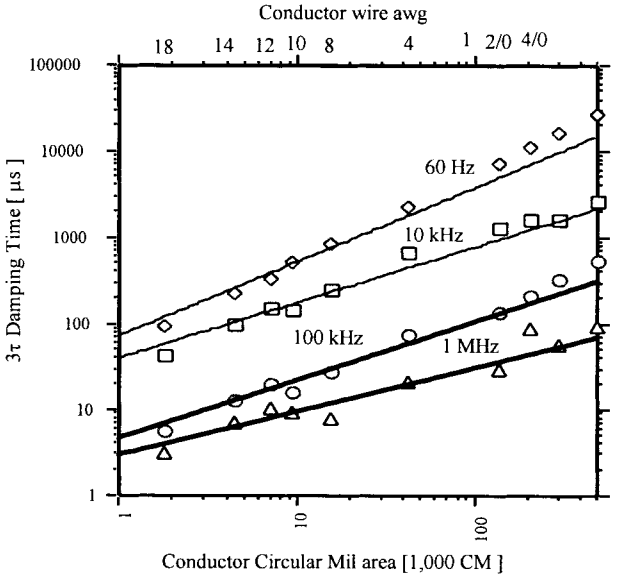

Fig. 6. Calculated 3τ damping time of reflected wave transient for PVC bundled conductor cables.

are short or if carrier frequency is increased, thus, reducing allowable decay times.

Low horsepower ac drives have small cable diameters, thus, have a reflection coefficient approximately equal to one ($\Gamma_m \approx$ 1), so that the predominant mechanism of transient overvoltage decay is through skin effect cable resistance damping. High horsepower ac drives have large cable diameters, so overvoltage transient decay from skin effect cable resistance damping in Fig. 6 is minimal. Luckily, these drives have reduced cable to motor Γ_m coefficients (<0.9). Thus, the main damping of the reflected waves is obtained by multiplying the reflected wave by these reduced Γ_m values at each successive f_o cycle until the transient decays. The breakpoint between these two different decay modes is thought to be somewhere in the vicinity of drive horsepowers using #8-AWG wire.

C. Summary

Existing literature on the effects of long cables emphasize the traditional 2-pu motor terminal voltage. Recent investigations have shown IGBT inverters induce motor overvoltages at 50 ft. This section of the paper has presented experimental data demonstrating >2-pu motor terminal voltages. The importance of *cable natural oscillation frequency* (f_o) and its dependency on cable length were presented and experimentally verified. *Cable damping time* (τ) *and its inverse relationship to* $\sqrt{f_o}$ *was theoretically established and confirmed with experimental results*.

IV. THE CONTRIBUTION OF MODULATORS TO MOTOR OVERVOLTAGE >2-PU BUS VOLTAGE

Investigations into motor overvoltages caused by IGBT inverters and long cable lengths generally focus on occurrences of motor voltages <2-pu. Although a few investigators have mentioned the possibility of >2-pu overvoltage, the majority do not explore the contributing factors and consider >2-pu bus

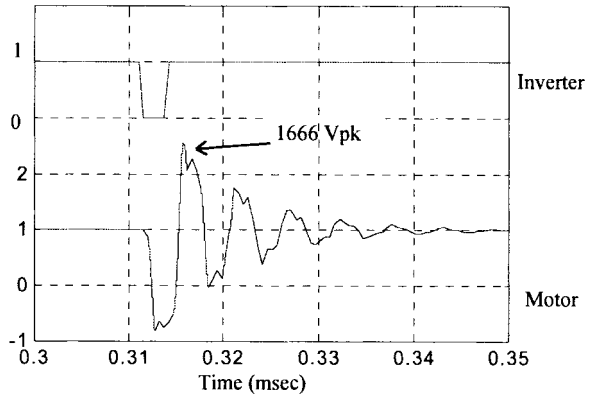

Fig. 7. Simulation of Fig. 3 (1 pu = 650 V).

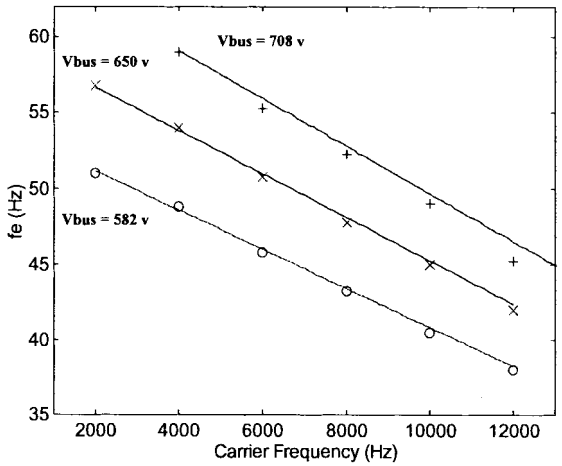

Fig. 8. Double pulsing inception frequency for TPWM (12 μs dwell time; high, nominal, low bus voltages, simulation versus experimental).

voltage not likely and, therefore, of little practical significance [4], [6], [9]–[15]. Recent motor winding failures precipitated an investigation into the exact nature of the mechanism responsible for motor winding degradation [5]. This investigation discovered motor terminal voltages exceeding two times the bus voltage are very probable. Further field experience and laboratory testing confirmed these findings.

A. Motor Voltages in Excess of 2 Times Bus Voltage Caused by Insufficient Dwell Time: The Double Pulsing Effect

1) Experimental Evidence: Fig. 3 demonstrates the >2-pu overvoltage phenomenon. This figure displays the inverter and motor line-to-line voltage for an unloaded 10-hp ac induction motor at 60 Hz. The drive employed a uniform sampled third-harmonic PWM (TPWM) modulator and a 4-kHz carrier. A 500-ft #12-gauge cable connected the drive to the motor.

Initially, the cable was in a fully charged condition $[V_i(0) = V_m(0) = V_{\rm bus}]$. A transient disturbance occurs $[V_i(1) = V_i(2) = V_i(3) = 0]$ by discharging the cable for approximately 4 μs (< dwell time, T_α). The propagation delay between the inverter terminals and motor terminals is fully recognizable and is approximately 1 μs. As is evident from the data, the reflection coefficient is nearly unity, thus, reflecting the incoming negative voltage and forcing the terminal voltage to approximately negative bus voltage $[V_m(1t_p) = V_m(0) - V_{\rm bus}(1 + \Gamma_m) \approx -V_{\rm bus}]$. A reflected wave $(-\Gamma_m V_{\rm bus})$ traveling from the motor to the inverter and back requires 2 μs. Prior to the arrival of the reflected wave, the terminal voltage tracks the characteristic response of the motor cable combination $[V_m(2t_p) \approx V_m(1t_p)]$. With the reflection coefficient of the inverter approximately -1 the reflected wave arrives at the motor terminals $[V_m(3t_p) = V_m(2t_p) - V_{\rm bus}\Gamma_i\Gamma_m(1+\Gamma_m) \approx V_{\rm bus}]$. The reflected wave $(-\Gamma_i\Gamma_m^2 V_{\rm bus})$ travels from the motor to the inverter where it is reflected and sent back to the motor $(-\Gamma_i^2\Gamma_m^2 V_{\rm bus})$. While this is occurring, $V_m(4t_p) \approx V_m(3t_p)$. In addition, at precisely the instant this reflected wave arrives at the motor terminals, the control's pulse $[V_i(4) = V_{\rm bus}]$ arrives. This new pulse is reflected by the motor, with the motor terminal voltage now achieving a peak value of 1670 $V_{\rm pk}$ $[V_m(5t_p) = V_m(4t_p) - (\Gamma_i^2\Gamma_m^2 V_{\rm bus}) + V_i(4)(1 + \Gamma_m) > 2V_{\rm bus}$ for $\Gamma_m < 1]$.

The above sequence of events may be referred to as *double pulsing* of a charged motor drive cable system. This contrasts with the single pulsing of charged or uncharged cables, as shown in Fig. 1, the voltage of which is limited to 2 times the bus voltage. The amplitude of the double-pulsed motor overvoltage, however, is governed by a number of variables. Obvious ones include the damping characteristics of the cable, bus voltage, and dwell time of the pulse. *Not as obvious, but perhaps more important, are carrier frequency, modulation technique, and duty cycle.*

2) Simulation Results: Cable parameters were calculated and correlated to typical cables employed in the industry. The parameters were combined with surge impedance values for ac induction motors and simulation studies performed. By varying cable lengths, device rise and fall times, load surge impedance, and control variables, including modulation technique, predictions were made of the motor terminal voltage. Fig. 7 shows simulation results for the conditions presented in Fig. 3. The simulation predicts a peak motor voltage of 1666 $V_{\rm pk}$ with a dominant frequency of approximately 180 kHz and 22 μs to damp within 5% of bus voltage. This compares favorably with the experimental results, which showed a peak voltage of 1670 $V_{\rm pk}$, a frequency of 200 kHz, and 23 μs.

3) Effects of Carrier Frequency and Modulator on Motor Overvoltage: With the existence of >2-pu voltage established, it is important to understand what contributes to the phenomenon. Clearly, damping characteristics of the cable, bus voltage, and dwell time are major contributors. However, double-pulsed overvoltages depend on carrier frequency, modulation strategy, and bus voltage [16]. Fig. 8 plots the operating frequency fe_α^*, at which double pulsing begins, as a function of carrier frequency and bus voltage for a TPWM modulator. This frequency, the *double pulsing inception frequency*, also depends on the type of modulation—sinewave, third-harmonic, space-vector, or two-phase [16].

Two items are apparent: first, for a fixed bus voltage, the operating frequency at which inception occurs decreases with increasing carrier frequency. Second, as the bus voltage increases, the inception frequency increases for a fixed carrier frequency. This result, although contrary to those of [12] and

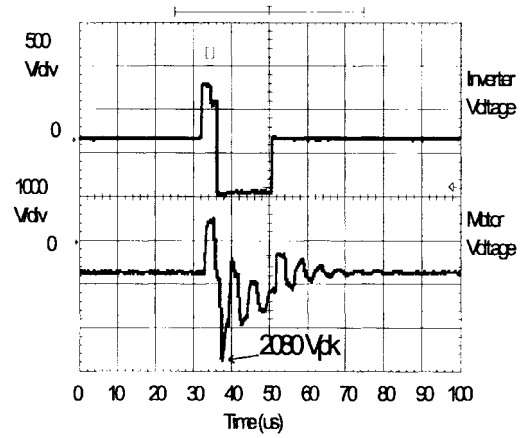

Fig. 9. Effect of polarity reversal.

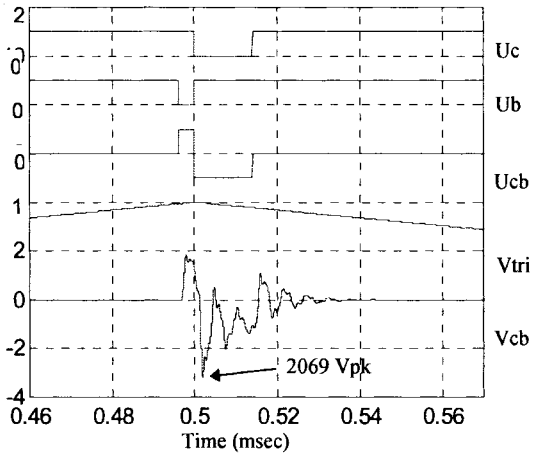

Fig. 10. Simulation of polarity reversal: expanded (1 pu = 650 V).

[14], clarifies the contribution of carrier frequency to excessive motor overvoltages. Increasing the carrier frequency increases the occurrences of double pulsing. Increased double pulsing, combined with insufficient dwell time T_α, provides a scenario for >2-pu.

B. Motor Overvoltages Due to Polarity Reversals: A New Contributor to Reflected Waves

Other investigators have discussed the existence of overvoltages >2-pu induced by double pulsing [13], [14]. However, another cause, referred to by the authors as *polarity reversal*, has not received comparable attention. *Polarity reversals* occur when the modulating signals are transitioning into and out of overmodulation or at the point of intersection of the two modulating waveforms.

1) Experimental Evidence: Fig. 9 shows the inverter and motor line-to-line voltages for a TPWM ac inverter drive with a 4-kHz carrier and a 10-hp 460-Vac induction motor operating at no load and 60 Hz. At bus voltages less than 640 V, TPWM's enter into overmodulation to maintain rated voltage. For the results of Fig. 9, the bus voltage was reduced to force overmodulation. As the modulating signals transition into and out of overmodulation, the line-to-line inverter voltage generates a *polarity reversal*. The resulting traveling wave excites an extreme voltage transient at the terminals of the machine. The measured voltage *exceeded 2000* $V_{\rm pk}$ *or 3-pu*. Voltages of this magnitude can *cause rapid motor winding failures*. Furthermore, at this level, even an inverter-rated motor's insulation level is exceeded [5].

2) Simulation Results: The simulation results displayed in Fig. 10 serve to explain the polarity reversal phenomena and also predict the tremendous overvoltages of Fig. 9. In this figure, two inverter phases U_c and U_b, the line-to-line voltage U_{cb}, the carrier V_{tri}, and the motor line-to-line voltage V_{cb}, are plotted. A 50-ns device rise time was employed in the simulation and is representative of the experimental results of Fig. 9. The line-to-line voltage, U_{cb}, displays the *polarity reversal*, the switching of the line-to-line voltage from plus $V_{\rm bus}$ to minus $V_{\rm bus}$.

As Fig. 10 shows, the predicted peak motor voltage, 2069 $V_{\rm pk}$, is in good agreement with the results of Fig. 9. Furthermore, the motor line voltage transient, both oscillation frequency (180 kHz) and 50% damping time (13 μs), compares favorably with the experimental result (200 kHz and 12 μs) of Fig. 9.

V. Restricting Motor Overvoltages >2-pu

Many approaches to limiting motor overvoltages <2-pu exist [4], [6], [9]–[18]. Thus far, these either incorporate passive filters with an attendant increase in drive cost or resort to limiting system parameters, e.g., IGBT rise time with the penalty of increasing switching losses [1]. This paper presents active and passive solutions to >2-pu overvoltage.

The first approach, the *pulse elimination technique (PET)*, modifies the PWM algorithm and prevents double pulsing and *polarity reversals*. The second approach, impedance matching technique, terminates the cable at the motor terminals with a passive load that matches the characteristic impedance of the cable. Other solutions, including both software and hardware corrections, may be found in [16].

A. Reducing Motor Overvoltages: The PET

1) Analysis: Fig. 11 shows a per phase block diagram of the PET. To facilitate an understanding of the functioning of the PET, reference is made to the pulse sequences of Fig. 12. The top trace depicts U_c transitioning out of overmodulation. The second trace shows U_b transitioning into overmodulation. The third trace is the line-to-line voltage U_{cb}. Note both a double pulsing and a polarity reversal are depicted. The bottom three traces show the same quantities after processing by the algorithm of Fig. 11.

First, the algorithm determines if a transition into the overmodulation region ($U_{\rm pwm} > T_c$) is occurring. If true, as shown in Fig. 12 for U_b, a counter is checked for a value N, the number of transition cycles. If the counter does not equal N, the counter is incremented and a maximum ($T_c - T_\alpha$) or minimum (T_α) T_{on} is maintained. This T_{on} is then processed for dead-time compensation prior to submittal to a digital comparator. If the counter equals N, then overmodulation is commenced and dead-time compensation not implemented.

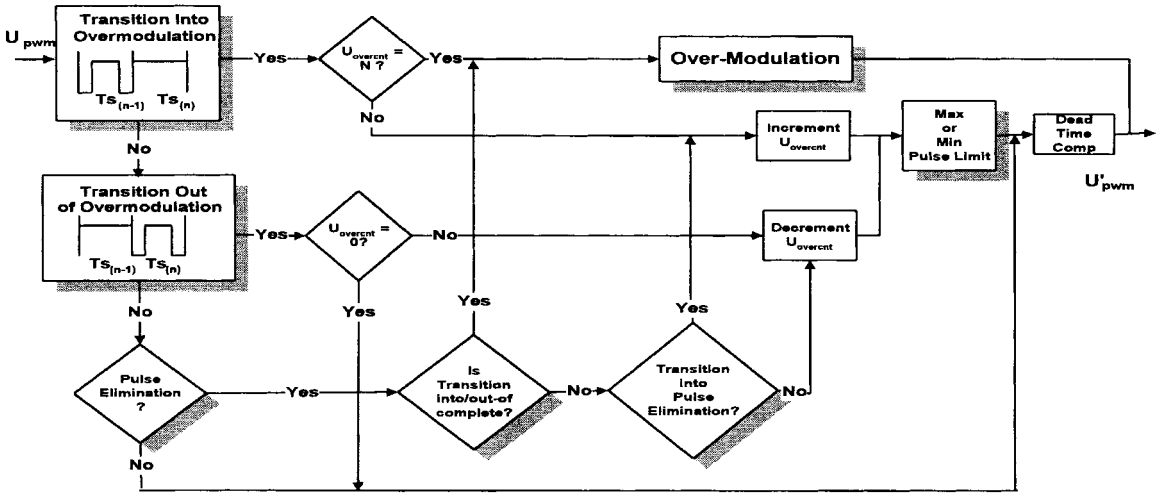

Fig. 11. Per phase block diagram for PET.

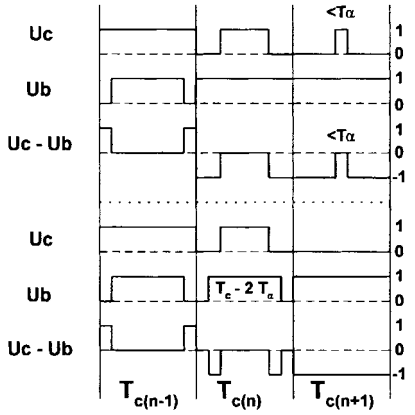

Fig. 12. Processing of pulse sequences by PET.

If a transition exists from the overmodulation region, U_c for example, then the counter is examined for a zero condition. If the counter is nonzero, the counter decrements and a maximum ($T_c - T_\alpha$) or minimum (T_α) T_{on} is executed prior to processing by the dead-time compensation. If the counter is zero, transition from overmodulation is completed and pulse time is processed for dead-time compensation. By ensuring the number of decrements equals the number of increments above, the volt seconds are symmetrically placed. The pulse elimination feature compensates for the reduction of the fundamental voltage caused by the volt-second placement.

Finally, if neither of the above conditions are met, the algorithm checks for double pulsing ($T_{on} < T_\alpha$ or $T_{on} > T_c - T_\alpha$). If true and transitioning is complete, the *pulse is eliminated* and the overmodulation algorithm is executed. In this manner, both *double pulsing* and *polarity reversals* are eliminated, without significantly affecting the fundamental voltage or harmonic content.

2) Experimental Evaluation: The algorithm was implemented in an Intel 80C196MC microprocessor. A TPWM provided the modulation strategy. Experimental evaluations were performed over the operating regions expected of

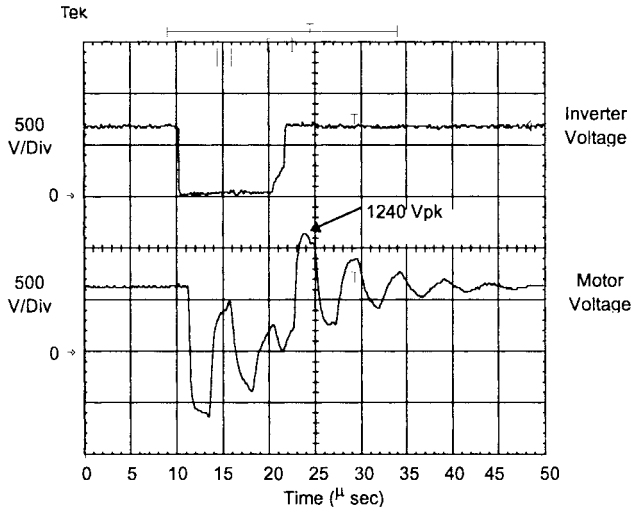

(a)

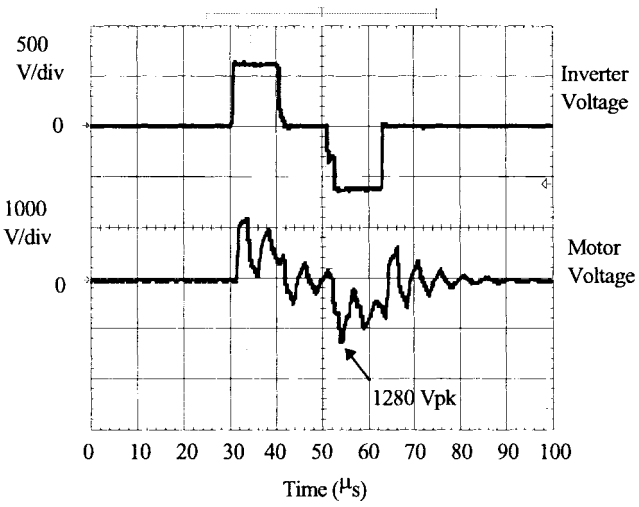

(b)

Fig. 13. (a) Fig. 3 with pulse elimination. (b) Fig. 5 with polarity reversal correction.

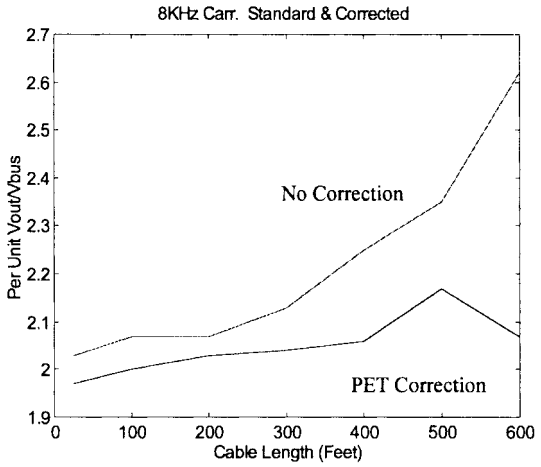

Fig. 14. Per unit data—no correction and PET correction.

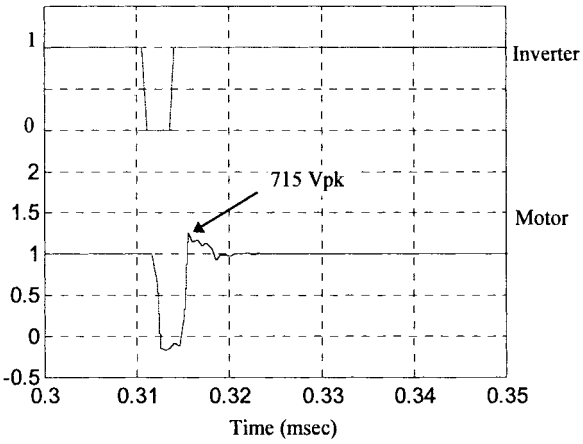

Fig. 15. Simulation of termination impedance.

industrial ac drives. Typical results are presented in Fig. 13 with the operating conditions the same as Figs. 3 and 9.

The oscilloscope was triggered on the motor line voltage with the level selected to trap the largest positive and negative value. Comparing the results, the PET with $T_\alpha = 12\ \mu$s, reduces the peak motor voltage from 1670 V_{pk} in the *double pulsing* mode of Fig. 3, to 1240 V_{pk} [Fig. 13(a)] transitioning into *pulse elimination* of Fig. 12. For polarity reversals, PET reduces the maximum voltage from 2080 V_{pk} (Fig. 9) to 1280 V_{pk} [Fig. 13(b)]. These reductions, to approximately 2-pu, were accomplished without significantly increasing the subcarrier harmonic content or the fundamental component of the applied voltage. Fig. 14 shows the per unit motor voltage as a function of cable length for both standard PWM and PET PWM. The operating conditions were 60 Hz, no load, 8-kHz carrier, and 650-Vdc bus. *The improvement provided by PET is substantial and maintains terminal voltage within inverter-grade motor ratings*.

By lowering the motor overvoltage to roughly 2-pu through modifications in the pulsewidth modulator, other elements incorporated in the system, such as filters, increased device rise time, and inline reactors, now are designed with a lower voltage objective. This reduces component size for the passive solutions and allows faster power device rise times, thus, retaining the benefits of reduced switching losses with high carrier frequencies without adverse motor overvoltages. Furthermore, restricting motor overvoltage to <1600 V_{pk} will ensure inverter-grade motors need not be derated.

B. Reducing Motor Overvoltage: Impedance Matching

Passive solutions to the overvoltage problem focus on inserting line reactors or incorporating filters. The line reactors reduce the steep wave fronts presented by the inverter, thereby attenuating the high-frequency components of the impressed voltage of Fig. 4. This solution can result in per-unit series impedance of up to 3%, with their accompanying fundamental voltage drop; thus, the available motor line voltage and deliverable torque are reduced [14]. Most filter proposals attempt to provide an overdamped or critically damped characteristic; however, the filter's performance depends on cable length, making the filter design application dependent, and neglects the effects of *double pulsing* and *polarity reversal* [10].

Another approach matches the load impedance to the characteristic impedance of the power cables [17]–[19]. Because the characteristic impedance of a low horsepower motor is much greater than typical cable characteristic impedance, a termination impedance matched to the cable when placed in parallel at the motor's terminals will provide a load impedance that approximates the cable's characteristic impedance. This will all but eliminate the reflected voltage wave and limit the motor voltage to $\approx V_{\text{bus}}$. Unlike a filter, the termination impedance is based on the cable characteristic impedance and is independent of cable length.

1) Simulation Results: Fig. 15 shows the motor's line-to-line voltage in response to an excitation identical to that of Fig. 7. In this case, however, a termination impedance equal to the cable characteristic impedance was added in parallel with the motor. Z_o was $\approx 87\ \Omega$ for the cable and $\approx 1000\ \Omega$ for the induction motor. Because of the substantial mismatch between cable and motor, the termination impedance dominates and essentially presents a matched load to traveling waves. Notice the peak voltage is now just 715 V_{pk}, slightly larger than the 650-V bus.

2) Experimental Results: A termination impedance consisting of a line-to-line series combination of resistance and capacitance was designed for #12-gauge cable. The cable's per unit length parameters were: $R_{\text{dc}} = 5.4 * 10^{-3}\ \Omega$/m, $C_o = 106$ pF/m, and $L_o = 780$ nH/m. Incorporating the skin-effect factor, the cable's $Z_o \cong 85\ \Omega$. For #12-gauge cable, therefore, the termination impedance (R_t and C_t) should approximate the cable's Z_o; thus, $R_t = 85\ \Omega$. The selection of the capacitance is governed by two main factors: limiting the voltage overshoot and ensuring discharge of the capacitance during the dwell time. With the PWM enhancements of PET, T_α is known, which allows for an optimization of the termination impedance. For the results presented in this paper, $C_t = 0.047\ \mu$F.

Fig. 16 shows the inverter and motor line-to-line voltages with an 8-kHz carrier frequency for the motor drive system

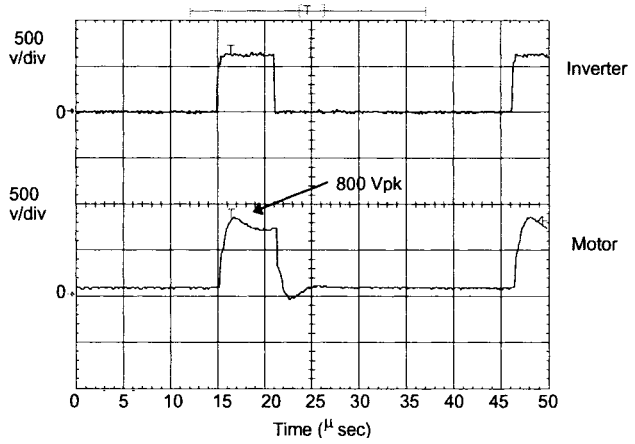

Fig. 16. Motor terminal voltage with termination impedance at 8 kHz.

of Figs. 3 and 9, with a termination impedance placed at the motor terminals. The results displayed do not incorporate PET, thus, displaying the improvement obtainable with passive filtering. The peak voltage is now limited to 800 V_{pk} at 8 kHz.

Fig. 4 includes results for a number of passive solutions. Inserting a series reactor at the inverter reduced the overvoltage by 33%. By moving the reactor to the motor terminals, the overvoltage is reduced by 38%. *However, with the termination impedance, the overvoltage is reduced by 50%, maintaining the motor terminal voltage within the guidelines for standard ac induction motors.*

Passive corrections, while solutions to motor overvoltages and field retrofitable, have limitations. The losses establish the physical size of the termination impedance and at low horsepowers result in relatively large and costly systems. Furthermore, the carrier frequency of the drive is limited because of heat dissipation in the termination block. However, experience has shown the termination impedance protects the motor when correctly applied.

VI. Conclusion

In this paper, motor overvoltage transients are investigated. The paper reports on two levels of motor overvoltage, <2-pu and >2-pu. A critical distance is developed, beyond which motor overvoltages >2-pu are likely. Contributing factors to <2-pu voltage, motor–cable impedance mismatch, power device rise time, and cable length, are discussed. The paper presents experimental data showing the tremendous voltages possible with modern IGBT inverters. Factors inducing >2-pu motor overvoltage are presented, including high-frequency cable damping, and PWM pulse patterns. PWM patterns, *double pulsing and polarity reversal*, are identified and correlated to carrier frequency, bus voltage, and modulation strategy. Solutions to motor overvoltages proposed in the paper include the following, which may be implemented independently or in combination: the *pulse elimination technique (PET)*, an active approach, and termination impedance matching, a passive approach.

Major findings reported in the paper are: 1) the importance of *cable natural oscillation frequency* (f_o), in addition to device rise time-related excitation frequency in determining maximum motor terminal voltage; 2) *cable damping time* (τ) is a significant factor in determining motor overvoltage and is a function of f_o; 3) the discovery of line-to-line voltage *polarity reversal* as a new contributor to motor overvoltage; 4) PWM carrier frequency influences motor overvoltage through the dwell time in double pulsing; and 5) the type of modulator establishes the operating regions where motor overvoltage is of concern.

References

[1] S. Evon, D. Kempke, L. Saunders, and G. Skibinski, "IGBT drive technology demands new motor and cable considerations," presented at the IEEE Petroleum and Chemical Industry Tech. Conf., Philadelphia, PA, Sept. 1996.
[2] E. Persson, "Transient effects in application of PWM inverters to induction motors," *IEEE Trans. Ind. Applicat.*, vol. 28, pp. 1095–1101, Sept./Oct. 1992.
[3] W. H. Hayt, *Engineering Electromagnetics.* New York: McGraw-Hill, 1989.
[4] Takahashi, M. Termeyer, T. Lowery, and H. Tsai, "Motor lead length issues for IGBT drives," in *Proc. IEEE Pulp and Paper Industry Conf.*, Vancouver, B.C., Canada, 1995, pp. 21–27.
[5] G. Skibinski, J. Erdman, and J. Pankau, "Assessing AC motor dielectric withstand capability to reflected voltage stress using corona testers," in *Proc. IEEE IAS Electric Machines Conf.*, San Diego, CA, 1996, pp. 694–702.
[6] S. Van Haute, A. Malfait, R. Reekmans, and R. Belmans, "Losses, audible noise, and overvoltage in induction motor drives," in *Proc. IEEE PESC,* 1995, pp. 585–592.
[7] G. Skibinski, D. Leggate, and R. J. Kerkman, "Cable characteristics and their influence on motor over-voltages," unpublished.
[8] G.L. Skibinski and D. M. Divan, "Design methodology & modeling of low inductance planar bus structures," in *Proc. EPE Conf.,* Brighton, U.K., 1993, pp. 98–105.
[9] L. Gubbala, A. von Jouanne, P. Enjeti, C. Singh, and H. Toliyat, "Voltage distribution in the windings of an AC motor subjected to high dv/dt PWM voltages," in *Proc. IEEE PESC Conf.*, 1995, pp. 579–585.
[10] A. von Jouanne and P. Enjeti, "Design considerations for an inverter output filter to mitigate the effects of long motor leads in ASD applications," in *Proc. IEEE IAS Conf.*, 1996, pp. 579–585.
[11] A. von Jouanne, P. Enjeti, and W. Gray, "The effect of long motor leads on PWM inverter fed AC motor drive systems," in *Proc. IEEE APEC,* 1995, pp. 592–597.
[12] P. Van Paucke, R. Belmans, W. Geysen, and E. Ternier, "Overvoltages in inverter fed induction machines using high frequency power electronic components," in *Proc. IEEE APEC Conf.*, 1994, pp. 536–541.
[13] C. J. Melhorn and L. Tang, "Transient effects of PWM ASD's on standard squirrel cage induction motors," in *Proc. IEEE IAS Conf.*, 1995, pp. 2689–2695.
[14] B. Kawkabani, J. J. Simond, and F. Kehtari, "Voltage peaks of low voltage motors due to PWM inverter supply," in *Proc. EPE Conf.*, Sevilla, Spain, 1995, pp. 465–469.
[15] B. Mokrytzki, "Filters for adjustable frequency drives," in *Proc. IEEE APEC Conf.*, 1994, pp. 542–548.
[16] R. J. Kerkman, D. Leggate, and G. Skibinski, "PWM inverters and their influence on motor over-voltages," unpublished.
[17] G. Skibinski, "Apparatus used with AC motors for eliminating line voltage reflections," U.S. Patent pending.
[18] A. von Jouanne, D. Rendusara, P. Enjeti, and W. Gray, "Filtering techniques to minimize the effect of long motor leads on PWM inverter fed AC motor drive systems," in *Proc. IEEE IAS Conf.*, 1995, pp. 37–44.
[19] G. Skibinski, "Design methodology of a cable terminator to reduce reflected voltage on ac motors," in *Proc. IEEE IAS Electric Machines Conf.,* San Diego, CA, 1996, pp.153–161.

Russel J. Kerkman (S'67–M'76–SM'87), for a photograph and biography, see p. 576 of the March/April 1997 issue of this Transactions.

David Leggate (S'90–M'93) received the B.S.E.E. degree from the Milwaukee School of Engineering, Milwaukee, WI, in 1992.

He has been with Rockwell Automation–Allen Bradley Company, Inc., Mequon, WI, since 1980, where he is currently a Senior Development Engineer. He has contributed to improvements in the design and development of ac induction motor drives. His current interests are in the development of control algorithms for general purpose ac industrial drives.

Gary L. Skibinski (M'96), for a photograph and biography, see p. 576 of the March/April 1997 issue of this TRANSACTIONS.